VGGT4D: Mining Motion Cues in Visual Geometry Transformers for 4D Scene Reconstruction

Yu Hu^{1*} Chong Cheng^{1,2*} Sicheng Yu^{1*}
Xiaoyang Guo² Hao Wang^{1†}

¹The Hong Kong University of Science and Technology (Guangzhou)

²Horizon Robotics

Abstract

Reconstructing dynamic 4D scenes is challenging, as it requires robust disentanglement of dynamic objects from the static background. While 3D foundation models like VGGT provide accurate 3D geometry, their performance drops markedly when moving objects dominate. Existing 4D approaches often rely on external priors, heavy postoptimization, or require fine-tuning on 4D datasets. In this paper, we propose VGGT4D, a training-free framework that extends the 3D foundation model VGGT for robust 4D scene reconstruction. Our approach is motivated by the key finding that VGGT's global attention layers already implicitly encode rich, layer-wise dynamic cues. To obtain masks that decouple static and dynamic elements, we mine and amplify global dynamic cues via gram similarity and aggregate them across a temporal window. To further sharpen mask boundaries, we introduce a refinement strategy driven by projection gradient. We then integrate these precise masks into VGGT's early-stage inference, effectively mitigating motion interference in both pose estimation and geometric reconstruction. Across six datasets, our method achieves superior performance in dynamic object segmentation, camera pose estimation, and dense reconstruction. It also supports single-pass inference on sequences longer than 500 frames.

Project Page: https://3dagentworld.github.
io/vggt4d/

1. Introduction

Reconstructing 4D scenes with dynamic objects from visual inputs has been a challenging task. This is because moving objects not only degrade pose estimation but also interfere with the background geometry modeling, and their motion is often entangled with camera motion, which leads to se-

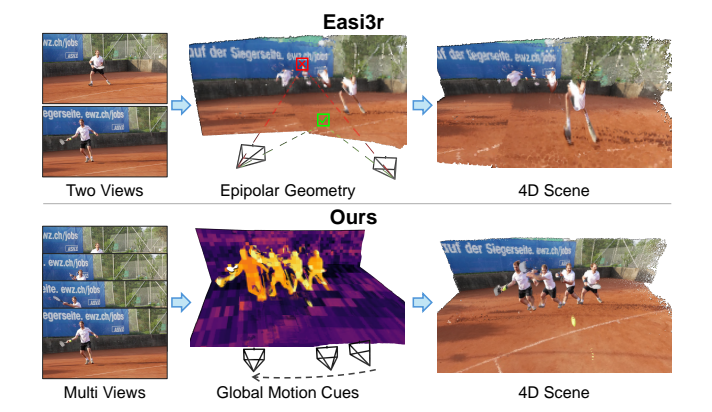


Figure 1. Easi3R, built upon DUSt3R, is restricted to twoview inputs and derives dynamic region masks by identifying epipolar-inconsistent pixels. In contrast, our proposed VGGT4D reconstructs dynamic scenes from multi-view inputs by extracting global motion cues from VGGT's attention maps.

vere artifacts in 3D scene representations. Therefore, how to model dynamics is crucial for robust 4D reconstruction.

Traditional SfM [2, 26] and MVS [10, 27] methods rely on multi-view rigidity and photometric constancy. Dynamic regions violate these assumptions, degrading correspondences and bundle adjustment, and often causing failure. 3D foundation models such as VGGT [32] deliver fast, accurate 3D geometry and camera pose estimation, yet they are largely trained and inferred under static-scene assumptions and lack an explicit mechanism to disentangle moving objects. When dynamics dominate, this coupling of dynamics and statics leads to brittle reconstruction and pose drift.

While existing methods have made progress in 4D reconstruction, they suffer from two limitations: (1) heavy iterative refinement that incurs substantial runtime and memory overhead [18, 40, 44]; (2) reliance on external modules (optical flow [41], depth [21], semantic segmentation [13]), which complicates integration and makes performance sensitive to module quality and domain shift. Recent efforts have explored efficient feed-forward archi-

^{*}Equal contribution.

[†]Corresponding author.

tectures [16, 33, 36, 37, 41, 42], but most still require large-scale training or fine-tuning on high-quality dynamic datasets, which are costly to curate and scarce at scale.

To alleviate the issues above, this paper aims to discover: can we endow 4D reconstruction capability to a 3D foundation model—without additional training?

A preliminary step toward this goal is Easi3R [6], a training-free extension of DUSt3R [34] that segments dynamic masks by analyzing the spatial and temporal statistics of decoder attention. However, Easi3R is built upon a pairwise cross-attention architecture, which captures only local feature interactions. This design imposes a short temporal horizon and yields masks that are inconsistent across frames, with boundary errors at dynamic–static interfaces that cause depth drift and floating artifacts in the reconstructed point clouds. Moreover, its core assumption that tokens violating epipolar geometry receive low attention does not generalize to VGGT, whose global attention aggregates signals across multiple views.

In this paper, we propose **VGGT4D**, which extends a pretrained VGGT model to 4D scene reconstruction without further retraining. Our design is motivated by empirical evidence of a consistent layer-wise trend in the original VGGT: shallow transformer layers capture salient motion information, which gradually fade in deeper layers.

Unlike Easi3R's pairwise attention statistics, our multiframe, layer-aware attention mining generalizes to VGGT and yields globally consistent, robust dynamic masks.

Specifically, we first derive per-frame dynamic masks by aggregating gram similarity statistics across selected shallow, middle, and deep layers and a temporal window, forming a dynamic saliency signal. This signal is then refined by a projection gradient-aware strategy, which yields sharp and robust masks that can explicitly decouple dynamic and static regions. Finally, during inference, we apply these masks by suppressing dynamic image tokens only in the shallow layers, which mitigates motion interference and yields undisturbed pose estimation and 4D reconstruction.

Experiments on six dynamic datasets demonstrate superior performance in dynamic-object segmentation, camera pose estimation, and dense point-cloud reconstruction, with the ability to process sequences of more than 500 frames in a single pass. The main contributions of this paper are summarized as follows:

- Training-free 4D perception for VGGT. We mine motion cues latent in VGGT's global attention to endow a 3D foundation model with 4D perception, without additional training.
- Consistent dynamic-static decoupling pipeline. We introduce a novel method that aggregates Gram similarity statistics from VGGT's attention and sharpens the resulting saliency signals with gradient-aware refinement, yielding masks that stabilize 4D reconstruction.

3. Superior Performance and Generalization. Our approach outperforms existing models on six dynamic datasets across dynamic segmentation, pose estimation, and 4D reconstruction. It also successfully processes long sequences (500+ frames) in a single pass.

2. Related Work

3D Foundation Models. DUSt3R [34] pioneered largescale pretraining for feed-forward 3D foundation models by predicting dense pointmaps from image pairs. MASt3R [20] strengthened correspondence quality, and Reloc3R [8] directly regressed 6-DoF poses to sharpen camera estimation. However, pairwise inputs make inference cost grow quadratically with sequence length. To lift this constraint, multi-image variants introduce memory encoders [5, 31] and subgraph fusion [22] to aggregate context without exhaustive pairing. VGGT [32] and Fast3R [38] further employ global attention for cross-view reasoning, while MV-DUSt3R+ [30] and FLARE [43] couple such priors with 3D Gaussian Splatting [17] for end-to-end reconstruction from sparse views. Recent follow-ups push beyond these methods with unified dense-geometry prediction [9], causal streaming for long sequences [19, 46], permutationequivariant, reference-free design [35], and training-free token-merging acceleration for VGGT [28]—delivering faster inference and stronger generalization.

4D Scene Reconstruction. Early methods often rely on RGB-D sensors, which limit applicability in real-world scenes [15, 24]. A large body of methods jointly estimate depth, pose, and residual motion (typically with a motion mask over stationary regions), including self-supervised variants [12, 14, 23, 39] and test-time or optimization-based schemes such as CasualSAM [44] and Robust-CVD [18]. More recent pipelines, e.g., MegaSaM [21], achieve robust poses and reconstructions on dynamic videos by leveraging strong monocular depth priors, while Uni4D [40] integrates multiple visual foundation models with multi-stage bundle adjustment for high-quality 4D results. These approaches are effective but hinge on strong priors and heavy test-time optimization, which limits scalability. Recent works reduce or replace test-time optimization using learned priors or attention adaptation: MonST3R [41] fine-tunes on dynamic data and exploits optical flow; DAS3R [37] augments a DPT head for feed-forward motion masks; CUT3R [33] fine-tunes MASt3R on mixed static/dynamic data for fast reconstruction; Easi3R [6] adapts attention during inference to perform training-free 4D reconstruction on DUSt3R. Despite the progress, most pipelines require fine-tuning or second-stage post-processing, and training-free variants are often tightly coupled to specific backbones and can become unstable on long sequences.

3. Method

3.1. Preliminary

DUSt3R. DUSt3R [34] is a pretrained transformer designed for pose-free dense 3D reconstruction. It processes only two input images and performs pairwise cross-attention to compute dense pixel-level correspondences between them.

Easi3R. Easi3R [6] extends DUSt3R to the task of 4D reconstruction. It leverages the empirical observation that DUSt3R assigns low attention to epipolar-inconsistent pixels, enabling Easi3R to derive dynamic region masks in an unsupervised manner from attention maps.

VGGT. VGGT [32] is an enhanced version of DUSt3R that processes multiple input images and jointly estimates multiview poses and dense geometry. It employs both inter-frame and intra-frame attention mechanisms, enabling tokens to aggregate semantically coherent evidence across frames for more consistent 3D reconstruction.

Motivation of our proposed VGGT4D. However, since Easi3R is built upon the DUSt3R framework, it is limited to pairwise image inputs and struggles to handle multi-view inputs effectively. To overcome this limitation, we propose VGGT4D, which extends VGGT from static multi-view reconstruction to 4D dynamic scene reconstruction.

3.2. Empirical Observations in VGGT

We first examine whether VGGT can perceive dynamic pixels. As illustrated in Fig. 3, we visualize the attention maps between the camera token and image tokens. The results reveal a clear separation between static and dynamic regions: shallow layers respond strongly to semantically dynamic objects (e.g., people), while deeper layers gradually suppress pixels with inconsistent multi-view geometry. These results suggest that VGGT is sensitive to physical motion and implicitly encodes dynamic cues.

However, this phenomenon is highly scene-dependent and occurs only at certain tokens and layers. Meanwhile, the attention maps among image tokens contain substantial high-level semantic noise, making direct extraction unreliable. To consistently and robustly identify dynamic object masks, we propose the following pipeline to achieve 4D reconstruction in a training-free manner.

3.3. Dynamic Cue Extraction via Gram Similarity

Easi3R [6] extracts dynamic masks directly from the standard attention map, given by

$$A_{l,t,s}^{QK} = \frac{Q_{l,t} K_{l,s}^{\top}}{\sqrt{c}} \in \mathbb{R}^{N_p \times N_p}, \tag{1}$$

where c is the feature dimension, l indexes the layer, t and s denote the frame indices, and N_p is the token count. However, we find that A^{QK} inherently mixes dynamic

motion with texture and semantic responses, thereby reduc-

ing the clarity of motion cues. To amplify the distribution discrepancies caused by motion, we propose to compute the Gram similarities QQ^{\top} and KK^{\top} :

$$A_{l,t,s}^{QQ} = \frac{Q_{l,t}Q_{l,s}^{\top}}{\sqrt{c}}, \quad A_{l,t,s}^{KK} = \frac{K_{l,t}K_{l,s}^{\top}}{\sqrt{c}}.$$
 (2)

These self-similarity matrices effectively enhance dynamic cues otherwise encoded implicitly within Q and K.

To aggregate temporal information, we employ an interframe sliding-window strategy across frames, defined as $W(t) = \{t - n, \dots, t - 1, t + 1, \dots, t + n\}.$ Within this window and across three set of layers L, including shallow, middle, and deep layers, we compute the mean (S) and variance (V) of the Gram similarities:

$$S_{i-j}^{\mathcal{X}} = \operatorname{Mean}_{s} \left(\frac{1}{|\mathcal{W}(t)|} \sum_{s \in \mathcal{W}(t)} \frac{1}{L} \sum_{l=i}^{j} A_{l,t,s}^{\mathcal{X}} \right), \quad (3)$$

$$V_{i-j}^{X} = \operatorname{Var}_{s} \left(\frac{1}{|\mathcal{W}(t)|} \sum_{s \in \mathcal{W}(t)} \frac{1}{L} \sum_{l=i}^{j} A_{l,t,s}^{X} \right), \quad (4)$$

where $X \in \{QQ, QK, KK\}$, i and j denote the start and end layer indices, respectively.

Finally, we construct a dynamic saliency map Dyn by mining these statistics:

$$Dyn = w_{shallow} \odot w_{middle} \odot w_{deep}, \tag{5}$$

where o denotes element-wise multiplication. The three factors capture complementary cues:

$$w_{\rm shallow} = (1 - S_{\rm shallow}^{KK}) \odot V_{\rm shallow}^{QK}, \tag{6} \label{eq:shallow}$$

$$w_{\text{middle}} = 1 - S_{\text{middle}}^{QQ},\tag{7}$$

$$w_{\text{middle}} = 1 - S_{\text{middle}}^{QQ},$$

$$w_{\text{deep}} = (1 - V_{\text{deep}}^{QQ}) \odot S_{\text{deep}}^{QQ}.$$
(8)

As illustrated in Fig. 4, $w_{\rm shallow}$ (shallow layers) captures semantic saliency, w_{middle} (middle layers) identifies motion instability, and $w_{\rm deep}$ (deep layers) acts as a spatial prior to suppress outliers. The per-frame dynamic mask is then obtained by thresholding, $M_t = [\mathrm{Dyn} > \alpha]$, and refined with feature clustering (see supplementary).

3.4. Mask Refinement via Projection Gradients

The masks extracted from ViT layers are coarse and lead to "floaters" in 4D reconstruction. Therefore, we propose a refinement method driven by point-cloud projection gradients to improve boundary accuracy.

Our core idea is that 3D points from dynamic objects will have large geometric and photometric errors when projected onto the *static* regions of other views. We first define a geometric loss for a 3D point projected onto view i:

$$\mathcal{L}_{proj} = \frac{1}{2} \mathbb{I}_i (1 - M_i) \|r_{d,i}\|_2^2,$$
 (9)

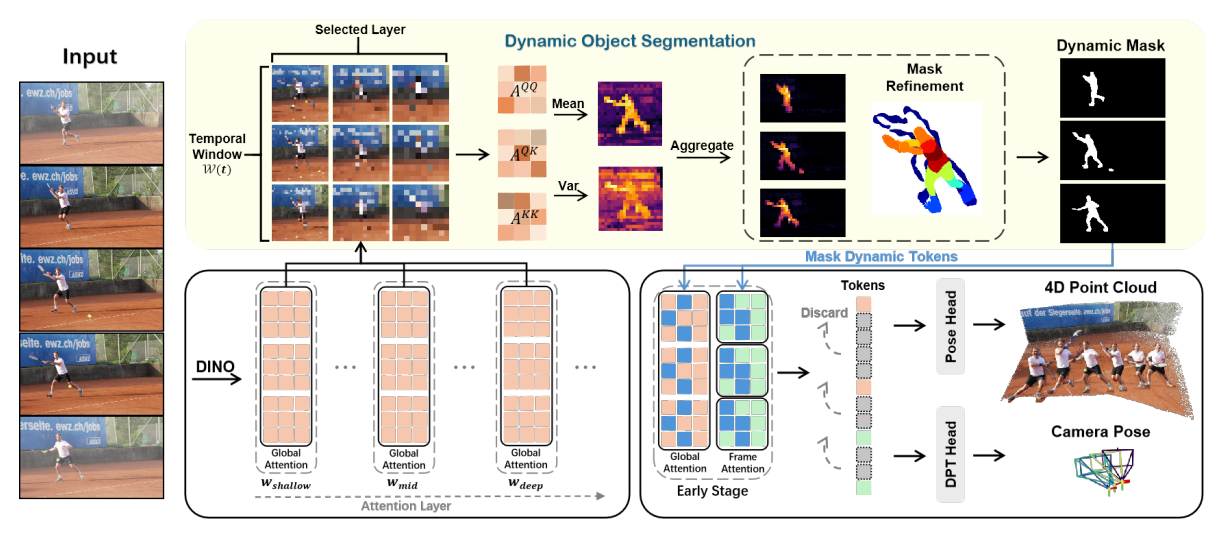


Figure 2. **Overview of VGGT4D.** Input image sequence is fed into VGGT. We compute and aggregate its global attention across selected layers and a temporal window to mine dynamic cues. Followed by a gradient-aware mask refinement, we get accurate dynamic masks. During inference, we apply the masks to early-stage layers and discard unused layer tokens, producing decoupled dynamic/static point clouds and camera pose estimates.

Method		DAVIS-2016			DAVIS-2017			DAVIS-all				
Wiemou	JM↑	JR↑	FM↑	FR↑	JM↑	JR↑	FM↑	FR↑	JM↑	JR↑	FM↑	FR↑
Easi3R _{dust3r}	50.10	55.77	43.40	37.25	46.86	50.54	39.06	30.05	44.10	50.85	35.16	27.24
Easi3R _{monst3r}	54.93	68.00	45.29	47.30	54.75	66.16	44.09	42.36	51.64	63.06	40.98	38.49
MonST3R	40.42	40.39	49.54	52.12	38.07	36.05	48.24	49.01	36.98	34.52	47.03	46.72
DAS3R	41.13	38.67	44.50	36.94	44.51	43.95	46.71	44.96	43.33	38.93	45.24	38.78
Ours	62.12	76.80	56.04	67.49	56.45	<u>65.62</u>	51.09	56.85	<u>50.75</u>	<u>55.59</u>	47.04	<u>46.43</u>

Table 1. **Dynamic object segmentation result on DAVIS dataset.** The best and second best results are **bold** and <u>underlined</u>, respectively. The subscript *DUSt3R/MonST3R* in Easi3R denotes the variant using the DUSt3R and MonST3R backbone.

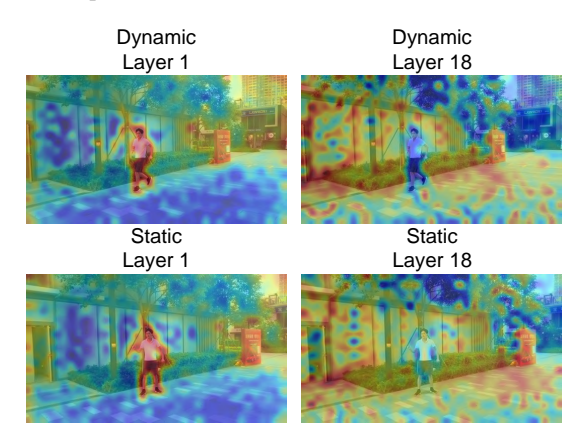


Figure 3. Visualization of VGGT's standard camera-image attention A^{QK} . At layer 1, attention strongly focuses on semantic regions (e.g., people). While deeper layers can suppress physically dynamic pixels, we observe this behavior is highly scene-dependent and unreliable for robust segmentation. This limitation motivates our search for a more stable dynamic cue (Sec. 3.3).

where $r_{d,i} = d_i - D_i(u_i, v_i)$, M_i is the initial dynamic mask, \mathbb{I}_i is the visibility mask, and $r_{d,i}$ is the depth residual between the projected depth d_i and the depth map D_i .

Points with large geometric gradients are likely dynamic. We compute the gradient of this residual $r_{d,i}$ with respect to the 3D point's coordinates. It is notable this gradient $\nabla r_{d,i}$ depends on the projection Jacobians and the spatial gradient of the target depth map.

To get a robust score, we aggregate these projection gradients across all N views:

$$\mathbf{agg}^{\text{proj}} = \frac{1}{N} \sum_{i}^{N} \left\| w_{i} \, r_{d,i} \, \nabla r_{d,i} \right\| ,$$
where $w_{i} = \mathbb{I}_{i} \left(1 - M_{i} \right)$. (10)

While the geometric gradient is effective, it can be unreliable in textureless regions (e.g., flat walls or floors) where depth gradients are uninformative. We therefore complement it with an aggregated photometric residual:

$$\mathbf{agg}^{\mathsf{photo}} = \frac{1}{N} \sum_{i}^{N} \left\| w_i \left(c - C_i(u_i, v_i) \right) \right\| , \qquad (11)$$

where c is the point's color and C_i is the sampled color in view i.

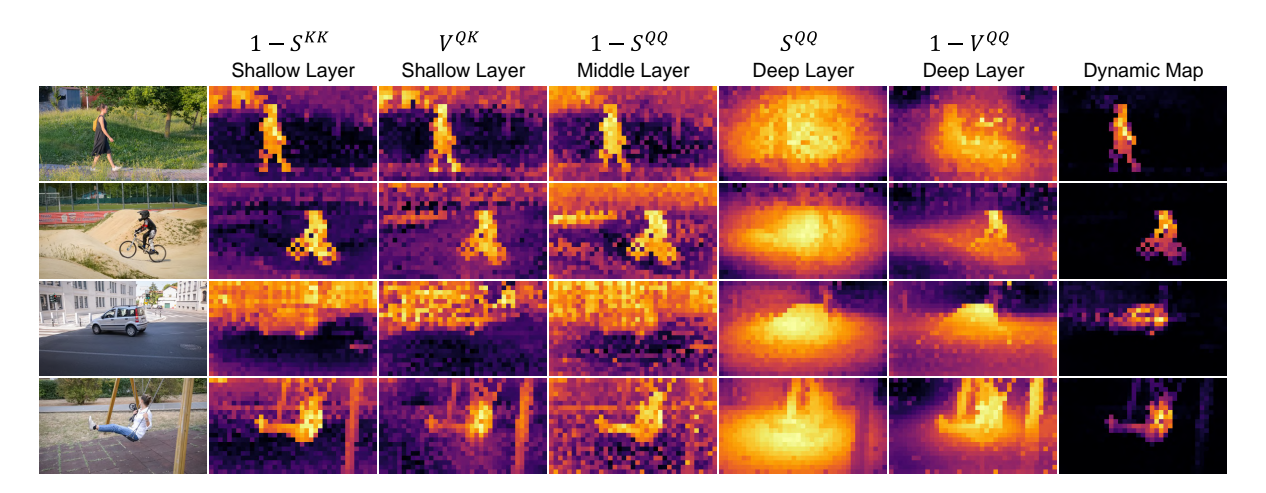


Figure 4. Visualization of gram similarity. We visualize each component of w_{shallow} , w_{middle} and w_{deep} across different layers, demonstrate their complementary roles in extracting dynamic cues.

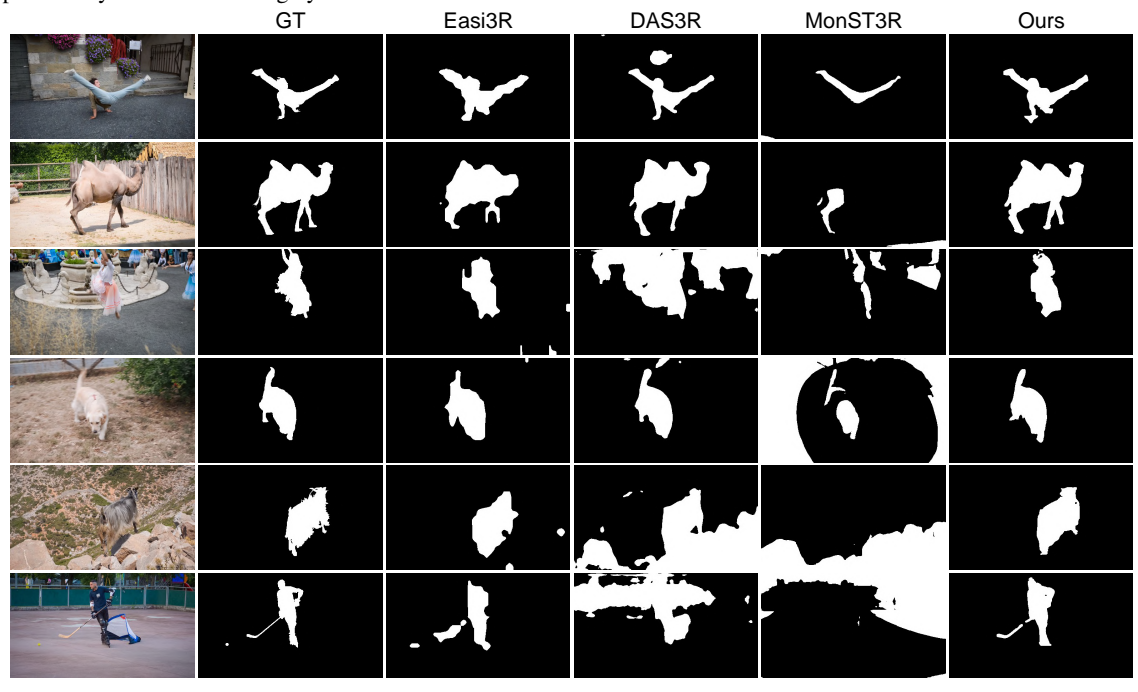


Figure 5. **Qualitative results of dynamic object segmentation.** Our method extracts sharp and accurate masks. In contrast, baseline methods suffer from coarse boundaries, missed details, and significant over-segmentation.

Finally, we combine these scores to re-classify the point:

$$\mathbf{agg}^{\text{total}} = \mathbf{agg}^{\text{proj}} + \lambda \mathbf{agg}^{\text{photo}}.$$
 (12)

A point is labeled dynamic if $\mathbf{agg}^{\mathrm{total}} > \tau$. This gradient-aware refinement effectively sharpens mask boundaries. We also apply point cloud filtering and spatial clustering for robustness (see supplementary).

3.5. 4D Reconstruction via Early-Stage Masking

With precise dynamic masks, we perform inference by integrating them into VGGT. This explicitly disentangles dynamic interference, enabling robust camera pose estimation and 4D point cloud reconstruction.

Dynamic pixels introduce geometric inconsistencies. However, naively masking all dynamic tokens in all layers is detrimental. VGGT already learns to partially attenuate dynamic signals; full-scale masking pushes the model into an out-of-distribution state, amplifying errors and removing valid static regions.

We propose a early-stage masking strategy. We mask dynamic image tokens only in the shallow semantic and midlevel layers (specifically, layers 1-5, see supplementary). We achieve this by suppressing the Key (K) vectors of dynamic tokens in these layers. This approach prevents dynamic information from contaminating the deeper geomet-

Method	Sintel			TUM-Dynamics			VKITTI		
	ATE↓	RTE↓	$RRE \downarrow$	ATE↓	RTE↓	RRE↓	ATE↓	RTE↓	RRE↓
Easi3R _{dust3r}	0.372	0.227	10.356	0.063	0.046	2.523	2.789	0.506	0.108
Easi3R _{monst3r}	0.109	0.051	0.277	0.133	0.120	4.366	2.036	0.173	0.124
MonST3R	0.151	0.034	0.258	0.156	0.103	12.041	2.272	0.180	0.091
POMATO	0.557	0.158	0.878	0.153	0.097	11.102	1.377	0.232	0.119
SpatialTrackerV2	0.073	0.035	0.340	0.054	0.041	2.530	0.720	0.160	0.127
DAS3R	0.125	0.030	0.185	0.155	0.102	12.038	2.043	0.169	0.114
CUT3R	0.152	0.077	0.454	0.054	0.041	5.346	5.583	0.381	0.174
VGGT	0.081	0.045	0.287	0.017	0.020	0.617	0.170	0.065	0.062
Ours	0.076	0.043	0.273	0.016	0.020	0.612	0.164	0.064	0.062

Table 2. **Quantitative comparisons of camera pose estimation.** Our method consistently improves upon the strong VGGT baseline and achieves SOTA results on the TUM-Dynamics and VKITTI datasets.

Method	ATE↓	RTE↓	RRE↓
Easi3R _{dust3r}	-	-	-
Easi3R _{monst3r}	-	-	-
MonST3R	-	-	-
POMATO	-	-	-
DAS3R	-	-	-
SpatialTrackerV2	-	-	-
CUT3R	0.417	0.028	0.605
FastVGGT	0.026	0.017	0.380
VGGT	0.022	<u>0.015</u>	<u>0.344</u>
Ours	0.019	0.009	0.290

Table 3. Quantitative comparisons of camera pose estimation on Point Odyssey dataset. Our method achieves the best accuracy while remaining highly efficient. Many specialized 4D methods fail with an out-of-memory (OOM) error ('-').

ric inference stages, while still allowing the deeper layers to operate within their trained distribution. This controlled intervention yields stable poses and clean, disentangled dynamic and static point clouds.

4. Experiments

Datasets. We assess dynamic mask estimation on the DAVIS [25] dataset. Camera pose estimation is evaluated on DyCheck [11], TUM-Dynamics [29], Sintel [3], VKITTI [4] and Point Odyssey [45], where we select several highly dynamic video sequences. For DyCheck, frames are sampled every 4 steps; for TUM-Dynamics, every 30 steps. Point cloud reconstruction is further evaluated on DyCheck. To measure long-sequence reconstruction, we use Point Odyssey [45] dataset with a sequence length of 500.

Baselines. We compare state-of-the-art pose-free 4D reconstruction methods, including MonST3R [41], DAS3R [37], CUT3R [33], Easi3R [6], SpatialTrackerV2 [36], and PO-MATO [42]. For long-sequence reconstruction, we also compare against FastVGGT [28].

Evaluation Metrics. For camera pose estimation, we use ATE, RTE, RRE. For point cloud reconstruction, we follow prior work [1, 7, 31] and measure Accuracy, Complete-

ness, and Distance, which are all distance-based metrics. For dynamic mask estimation, we use IoU and Boundary F-measure, first averaging within each sequence and then across sequences. These metrics are denoted as JM and FM, respectively. To assess recall, we define a successful retrieval when IoU or Boundary F-measure exceeds 0.5, and report the mean recalls JR and FR.

Implementation Details. All experiments are conducted on a single NVIDIA A6000 GPU. We also modify VGGT's attention operator. For more implementation details, please refer to the supplementary material.

Long-sequence Inference Implementation. To enable long-sequence inference, we build upon FastVGGT [28]. We leverage the finding that VGGT's prediction heads only consume tokens from specific layers, i.e., (5, 12, 18, 24). We therefore discard all intermediate tokens from other layers during inference. This significantly reduces the memory footprint, allowing our method to process sequences of over 500 frames on Point Odyssey [45]. Our dynamic token masking is applied on top of this efficient long-sequence backbone, bringing additional accuracy gains.

4.1. Dynamic Object Segmentation

We first evaluate the core component of our method: dynamic object segmentation. Results are presented in Tab. 1 and qualitatively in Fig. 5.

As shown in Tab. 1, our full method significantly outperforms all other variants, achieving SOTA performance on DAVIS-2016 and DAVIS-2017 datasets. The qualitative results in Fig. 5 provide a clear picture: Easi3R's masks are coarse and miss details. DAS3R [37] tends to over-segment, bleeding into the static background, while MonST3R [41] often under-segments, failing to capture entire moving parts. In contrast, our method produces masks that are both more accurate and have sharper boundaries.

These results demonstrate that **our dynamic-mining is effective**. The strong performance validates our hypothesis that rich, extractable motion cues are embedded within VGGT's Gram similarity statistics, even without any 4D-

Method	Pose Estimation		Accuracy		Completeness		Distance		
11101104	ATE↓	RTE↓	RRE↓	Mean↓	Median↓	Mean↓	Median↓	Mean↓	Median↓
Easi3R _{dust3r}	0.022	0.009	0.806	0.070	0.044	0.060	0.033	0.194	0.132
Easi3R _{monst3r}	0.032	0.008	1.075	0.100	0.050	0.121	0.082	0.289	0.270
MonST3R	0.038	0.010	1.172	0.090	0.033	0.113	0.064	0.279	0.234
POMATO	0.128	0.027	3.648	0.960	0.950	0.814	0.776	1.484	1.434
SpatialTrackerV2	0.011	0.006	0.347	0.115	0.064	0.052	0.026	0.421	0.304
DAS3R	0.052	0.012	1.560	0.192	0.142	0.250	0.108	0.428	0.336
CUT3R	0.036	0.013	0.860	0.073	0.054	0.133	0.049	0.328	0.224
VGGT	0.013	0.008	0.418	0.028	0.009	0.063	<u>0.019</u>	<u>0.150</u>	<u>0.055</u>
Ours	0.010	0.007	0.374	0.022	0.004	0.051	0.012	0.123	0.050

Table 4. Quantitative comparisons on DyCheck dataset. Our method achieves the best performance across all 4D reconstruction metrics. While SpatialTrackerV2 also shows strong pose results, its reconstruction quality is poor; our method excels in both tasks simultaneously.

specific training.

While $Easi3R_{monst3r}$ shows competitive recall on DAVISall, this stems from MonST3R's post-training on optical flow. Our method achieves its results in a training-free manner, operating solely on the pretrained VGGT model.

4.2. Camera Pose Estimation

We evaluate camera pose estimation on several standard and challenging dynamic datasets. The results are shown in Tabs. 2 to 4.

A key observation from the tables is that the original VGGT is already an exceptionally strong baseline, outperforming many specialized 4D reconstruction methods (e.g., MonST3R, DAS3R, CUT3R) on its own. This suggests its pretraining on diverse data implicitly taught it to be partially robust to dynamic objects.

However, this robustness is not perfect. Our method, VGGT4D consistently improves upon this strong VGGT baseline across all datasets. On the long-sequence Point Odyssey benchmark (Tab. 3), we achieve the best results in all metrics while remaining highly efficient. Many other 4D methods fail to even run on this 500-frame sequence due to OOM errors.

This demonstrates that VGGT's implicit compensation is incomplete. Our explicit, training-free dynamic-static decoupling successfully identifies and removes the residual pose inconsistencies caused by motion, leading to a more stable and accurate camera trajectory, especially on long and complex sequences.

4.3. 4D Reconstruction

We evaluate the final 4D point cloud reconstruction quality on the DyCheck dataset (Tab. 4) and present qualitative results in Fig. 6.

Quantitatively, our method achieves the best performance on all reconstruction metrics (Accuracy, Completeness, and Distance). The improvement over the strong VGGT baseline is significant, for example, reducing the median Accuracy error from 0.009 to 0.004 and the mean

Distance from 0.150 to 0.123.

These numbers are confirmed by the visual evidence in Fig. 6. Baselines like MonST3R and Easi3R produce noisy and artifact-ridden reconstructions. Dynamic objects are often "ghosted" across the static scene (rows 1, 2), and static backgrounds are fragmented (row 3). Our method, by contrast, generates a visibly cleaner static point cloud and more coherent, well-separated dynamic objects (e.g., the human in row 4).

This qualitative leap is a direct result of our complete pipeline: (1) Our accurate dynamic masks correctly identify the dynamic regions. (2) Our gradient-aware refinement ensures sharp boundaries, preventing background "floaters". (3) Our 'early-stage masking' strategy effectively prevents this dynamic information from contaminating the deep geometric reasoning layers, allowing for a clean separation.

4.4. Ablation Studies

We conduct two crucial ablation studies to validate our core design choices.

Dynamic Mask Estimation Ablation. In Tab. 5, we analyze the components of our mask generation pipeline on the DAVIS dataset.

- Easi3R's logic on VGGT fails. We first test Easi3R's epipolar-based method on VGGT backbone (Easi3R_{vggt}). The performance is poor. This empirically confirms our hypothesis: Easi3R's design is fundamentally incompatible with VGGT's global attention, which does not rely on simple pairwise epipolar geometry.
- Our Gram Similarity mining works. Our initial mask, generated purely from mining Gram similarities (w/o refine), already achieves a very strong 59.74 JM. This proves our core motion-mining technique is highly effective and far superior to the Easi3R baseline for this architecture.
- Refinement adds a critical boost. Adding our gradientbased refinement (Ours) provides the final, significant boost to 62.12 JM. This validates its role in removing static regions near motion boundaries and sharpening the

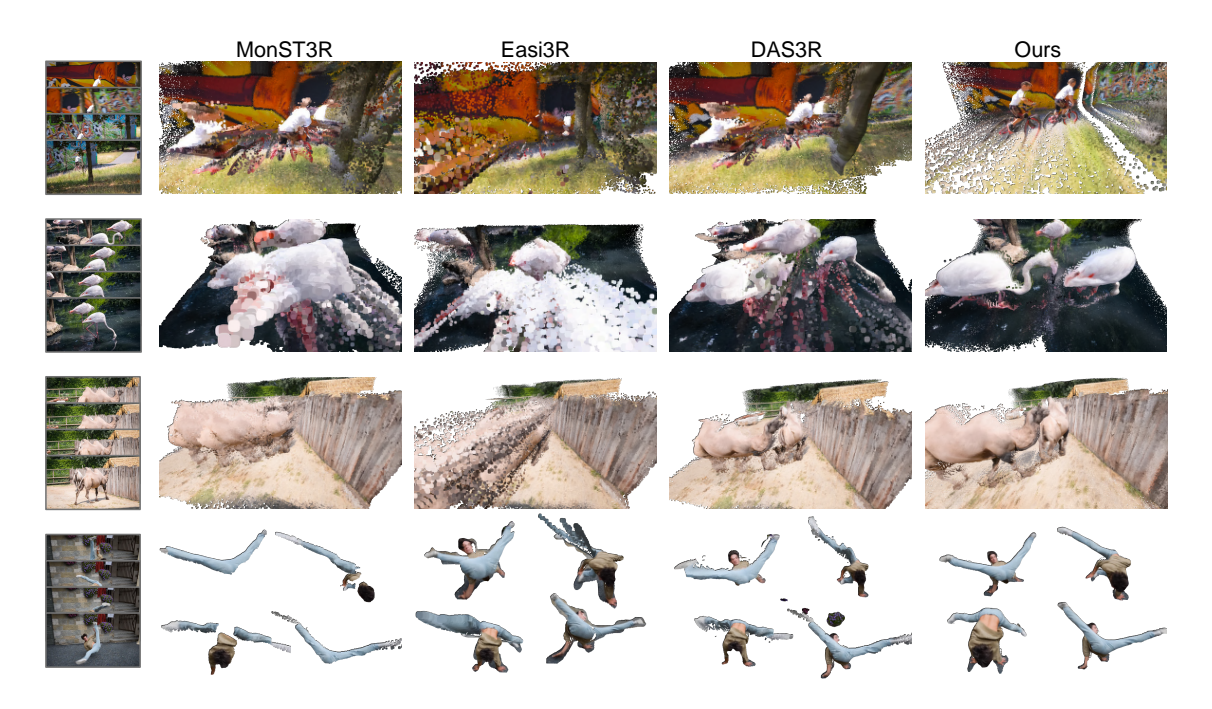


Figure 6. Qualitative comparisons of 4D reconstruction. Baselines exhibit significant artifacts and noisy static backgrounds due to poor dynamic-static separation. In contrast, our method produces cleaner static scenes and more coherent, well-separated dynamic objects.

Method		DAVIS	S-2016		DAVIS	S-2017		DAV	IS-all	
	JM↑	JR↑	FM↑	FR↑ JM↑	JR↑	FM↑	FR↑ JM↑	JR↑	FM↑	FR↑
Easi3R _{vggt}	7.51	0.12	12.78	0.00 10.61	0.08	16.73	0.08 10.58	0.12	17.36	0.24
w/o refine		73.10	50.64	58.30 54.26	62.72	46.37	47.32 47.71	50.39	40.00	32.40
Ours	62.12	76.80	56.04	67.49 56.45	65.62	51.09	56.85 50.75	55.59	47.04	46.43

Table 5. **Ablation on dynamic mask estimation.** We validate our design choices: (1) Easi3R's epipolar logic fails on VGGT ($Easi3R_{vggt}$), confirming its incompatibility. (2) Our core Gram similarity mining (w/o refine) is already highly effective. (3) The gradient-based refinement (Ours) provides a significant final boost by sharpening boundaries.

Method	ATE↓	RTE↓	RRE↓
Full Mask VGGT	0.0302 0.0131	0.0213 0.0082	1.0660 0.4185
Ours	0.0106	0.0072	0.3746

Table 6. **Ablation on attention mask on DyCheck dataset.** *Full Mask* denotes applying dynamic masks to all attention layers of VGGT and *Ours* refers to our proposed method.

final mask.

Pose Estimation Ablation. In Tab. 6, we analyze our early-stage masking strategy for pose estimation on DyCheck. We compare three variants: the baseline *VGGT* (no mask), a naive *Full Mask* (masking dynamic tokens in all layers), and *Ours* (selective 'early-stage' masking).

• Full Masking is harmful. Naively applying the mask in all layers is worse than using no mask at all (ATE 0.0302 vs. 0.0131). As hypothesized, this pushes the model into an out-of-distribution state and discards too much information.

Selective Masking is optimal. Our strategy achieves the
best performance (ATE 0.0106). This demonstrates that
VGGT benefits from controlled intervention. By only
suppressing dynamic tokens in the shallow and mid-level
layers, we prevent motion from corrupting the initial geometric features while allowing the deeper layers to operate within their trained distribution.

5. Conclusion

We present a training-free framework that extends VGGT to 4D scene reconstruction. We investigate VGGT's inherent ability to perceive dynamic objects. By leveraging Gram Similarity signals extracted from VGGT's attention, we mine and amplify dynamic cues, enabling explicit dynamic disentanglement without relying on any external segmentation modules. To sharpen dynamic masks, we apply a projection gradient based refinement strategy. We integrate the refined dynamic masks into VGGT's early inference, effectively suppressing dynamic interference and im-

proving both pose estimation and geometric reconstruction. Our method achieves superior quantitative performance and higher-quality visual results. We hope our findings offer insights for future research on 4D foundation models.

References

- [1] Henrik Aanæs, Rasmus Ramsbøl Jensen, George Vogiatzis, Engin Tola, and Anders Bjorholm Dahl. Large-scale data for multiple-view stereopsis. *International Journal of Computer Vision*, 120(2):153–168, 2016. 6
- [2] Sameer Agarwal, Yasutaka Furukawa, Noah Snavely, Ian Simon, Brian Curless, Steven M Seitz, and Richard Szeliski. Building rome in a day. *Communications of the ACM*, 54 (10):105–112, 2011.
- [3] D. J. Butler, J. Wulff, G. B. Stanley, and M. J. Black. A naturalistic open source movie for optical flow evaluation. In *European Conf. on Computer Vision (ECCV)*, pages 611–625. Springer-Verlag, 2012. 6
- [4] Yohann Cabon, Naila Murray, and Martin Humenberger. Virtual kitti 2, 2020.
- [5] Yohann Cabon, Lucas Stoffl, Leonid Antsfeld, Gabriela Csurka, Boris Chidlovskii, Jerome Revaud, and Vincent Leroy. Must3r: Multi-view network for stereo 3d reconstruction. In *Proceedings of the Computer Vision and Pattern Recognition Conference*, pages 1050–1060, 2025. 2
- [6] Xingyu Chen, Yue Chen, Yuliang Xiu, Andreas Geiger, and Anpei Chen. Easi3r: Estimating disentangled motion from dust3r without training. *arXiv preprint arXiv:2503.24391*, 2025. 2, 3, 6
- [7] Yue Chen, Xingyu Chen, Anpei Chen, Gerard Pons-Moll, and Yuliang Xiu. Feat2gs: Probing visual foundation models with gaussian splatting, 2024. 6
- [8] Siyan Dong, Shuzhe Wang, Shaohui Liu, Lulu Cai, Qingnan Fan, Juho Kannala, and Yanchao Yang. Reloc3r: Large-scale training of relative camera pose regression for generalizable, fast, and accurate visual localization. In *Proceedings of the Computer Vision and Pattern Recognition Conference*, pages 16739–16752, 2025.
- [9] Xianze Fang, Jingnan Gao, Zhe Wang, Zhuo Chen, Xingyu Ren, Jiangjing Lyu, Qiaomu Ren, Zhonglei Yang, Xiaokang Yang, Yichao Yan, et al. Dens3r: A foundation model for 3d geometry prediction. arXiv preprint arXiv:2507.16290, 2025. 2
- [10] Yasutaka Furukawa and Jean Ponce. Accurate, dense, and robust multiview stereopsis. *IEEE transactions on pattern* analysis and machine intelligence, 32(8):1362–1376, 2009.
- [11] Hang Gao, Ruilong Li, Shubham Tulsiani, Bryan Russell, and Angjoo Kanazawa. Monocular dynamic view synthesis: A reality check. In *NeurIPS*, 2022. 6
- [12] Clément Godard, Oisin Mac Aodha, Michael Firman, and Gabriel J Brostow. Digging into self-supervised monocular depth estimation. In *Proceedings of the IEEE/CVF inter*national conference on computer vision, pages 3828–3838, 2019. 2

- [13] Lily Goli, Sara Sabour, Mark Matthews, Marcus A Brubaker, Dmitry Lagun, Alec Jacobson, David J Fleet, Saurabh Saxena, and Andrea Tagliasacchi. Romo: Robust motion segmentation improves structure from motion. In *Proceedings* of the IEEE/CVF International Conference on Computer Vision, pages 6155–6164, 2025. 1
- [14] Ariel Gordon, Hanhan Li, Rico Jonschkowski, and Anelia Angelova. Depth from videos in the wild: Unsupervised monocular depth learning from unknown cameras. In *Pro*ceedings of the IEEE/CVF international conference on computer vision, pages 8977–8986, 2019. 2
- [15] Matthias Innmann, Michael Zollhöfer, Matthias Nießner, Christian Theobalt, and Marc Stamminger. Volumedeform: Real-time volumetric non-rigid reconstruction. In *European conference on computer vision*, pages 362–379. Springer, 2016. 2
- [16] Zeren Jiang, Chuanxia Zheng, Iro Laina, Diane Larlus, and Andrea Vedaldi. Geo4d: Leveraging video generators for geometric 4d scene reconstruction. arXiv preprint arXiv:2504.07961, 2025. 2
- [17] Bernhard Kerbl, Georgios Kopanas, Thomas Leimkühler, and George Drettakis. 3d gaussian splatting for real-time radiance field rendering. ACM Trans. Graph., 42(4):139–1, 2023. 2
- [18] Johannes Kopf, Xuejian Rong, and Jia-Bin Huang. Robust consistent video depth estimation. In *Proceedings of the IEEE/CVF Conference on Computer Vision and Pattern Recognition*, pages 1611–1621, 2021. 1, 2
- [19] Yushi Lan, Yihang Luo, Fangzhou Hong, Shangchen Zhou, Honghua Chen, Zhaoyang Lyu, Shuai Yang, Bo Dai, Chen Change Loy, and Xingang Pan. Stream3r: Scalable sequential 3d reconstruction with causal transformer. *arXiv* preprint arXiv:2508.10893, 2025. 2
- [20] Vincent Leroy, Yohann Cabon, and Jérôme Revaud. Grounding image matching in 3d with mast3r. In *European Conference on Computer Vision*, pages 71–91. Springer, 2024. 2
- [21] Zhengqi Li, Richard Tucker, Forrester Cole, Qianqian Wang, Linyi Jin, Vickie Ye, Angjoo Kanazawa, Aleksander Holynski, and Noah Snavely. Megasam: Accurate, fast and robust structure and motion from casual dynamic videos. In Proceedings of the Computer Vision and Pattern Recognition Conference, pages 10486–10496, 2025. 1, 2
- [22] Yuzheng Liu, Siyan Dong, Shuzhe Wang, Yingda Yin, Yanchao Yang, Qingnan Fan, and Baoquan Chen. Slam3r: Realtime dense scene reconstruction from monocular rgb videos. arXiv preprint arXiv:2412.09401, 2024. 2
- [23] Reza Mahjourian, Martin Wicke, and Anelia Angelova. Unsupervised learning of depth and ego-motion from monocular video using 3d geometric constraints. In *Proceedings of the IEEE conference on computer vision and pattern recognition*, pages 5667–5675, 2018. 2
- [24] Richard A Newcombe, Dieter Fox, and Steven M Seitz. Dynamicfusion: Reconstruction and tracking of non-rigid scenes in real-time. In *Proceedings of the IEEE conference* on computer vision and pattern recognition, pages 343–352, 2015.
- [25] F. Perazzi, J. Pont-Tuset, B. McWilliams, L. Van Gool, M. Gross, and A. Sorkine-Hornung. A benchmark dataset and

- evaluation methodology for video object segmentation. In *Computer Vision and Pattern Recognition*, 2016. 6
- [26] Johannes L Schonberger and Jan-Michael Frahm. Structurefrom-motion revisited. In *Proceedings of the IEEE con*ference on computer vision and pattern recognition, pages 4104–4113, 2016. 1
- [27] Johannes L Schönberger, Enliang Zheng, Jan-Michael Frahm, and Marc Pollefeys. Pixelwise view selection for unstructured multi-view stereo. In *European conference on computer vision*, pages 501–518. Springer, 2016. 1
- [28] You Shen, Zhipeng Zhang, Yansong Qu, and Liujuan Cao. Fastvggt: Training-free acceleration of visual geometry transformer. arXiv preprint arXiv:2509.02560, 2025. 2, 6
- [29] J. Sturm, N. Engelhard, F. Endres, W. Burgard, and D. Cremers. A benchmark for the evaluation of rgb-d slam systems. In *Proc. of the International Conference on Intelligent Robot Systems (IROS)*, 2012. 6
- [30] Zhenggang Tang, Yuchen Fan, Dilin Wang, Hongyu Xu, Rakesh Ranjan, Alexander Schwing, and Zhicheng Yan. Mv-dust3r+: Single-stage scene reconstruction from sparse views in 2 seconds. arXiv preprint arXiv:2412.06974, 2024.
- [31] Hengyi Wang and Lourdes Agapito. 3d reconstruction with spatial memory. arXiv preprint arXiv:2408.16061, 2024. 2,
- [32] Jianyuan Wang, Minghao Chen, Nikita Karaev, Andrea Vedaldi, Christian Rupprecht, and David Novotny. Vggt: Visual geometry grounded transformer. In Proceedings of the IEEE/CVF Conference on Computer Vision and Pattern Recognition, 2025. 1, 2, 3
- [33] Qianqian Wang, Yifei Zhang, Aleksander Holynski, Alexei A. Efros, and Angjoo Kanazawa. Continuous 3d perception model with persistent state. In CVPR, 2025. 2, 6
- [34] Shuzhe Wang, Vincent Leroy, Yohann Cabon, Boris Chidlovskii, and Jerome Revaud. Dust3r: Geometric 3d vision made easy. In CVPR, 2024. 2, 3
- [35] Yifan Wang, Jianjun Zhou, Haoyi Zhu, Wenzheng Chang, Yang Zhou, Zizun Li, Junyi Chen, Jiangmiao Pang, Chunhua Shen, and Tong He. π^3 : Scalable permutation-equivariant visual geometry learning. *arXiv preprint arXiv:2507.13347*, 2025. 2
- [36] Yuxi Xiao, Jianyuan Wang, Nan Xue, Nikita Karaev, Yuri Makarov, Bingyi Kang, Xing Zhu, Hujun Bao, Yujun Shen, and Xiaowei Zhou. Spatialtrackerv2: 3d point tracking made easy. arXiv preprint arXiv:2507.12462, 2025. 2, 6
- [37] Kai Xu, Tze Ho Elden Tse, Jizong Peng, and Angela Yao. Das3r: Dynamics-aware gaussian splatting for static scene reconstruction. *arXiv* preprint arxiv:2412.19584, 2024. 2, 6
- [38] Jianing Yang, Alexander Sax, Kevin J. Liang, Mikael Henaff, Hao Tang, Ang Cao, Joyce Chai, Franziska Meier, and Matt Feiszli. Fast3r: Towards 3d reconstruction of 1000+ images in one forward pass. In Proceedings of the IEEE/CVF Conference on Computer Vision and Pattern Recognition (CVPR), 2025. 2
- [39] Zhenheng Yang, Peng Wang, Yang Wang, Wei Xu, and Ram Nevatia. Every pixel counts: Unsupervised geometry learning with holistic 3d motion understanding. In *Proceedings of*

- the European conference on computer vision (ECCV) workshops, pages 0–0, 2018. 2
- [40] David Yifan Yao, Albert J Zhai, and Shenlong Wang. Uni4d: Unifying visual foundation models for 4d modeling from a single video. In *Proceedings of the Computer Vision and Pattern Recognition Conference*, pages 1116–1126, 2025. 1,
- [41] Junyi Zhang, Charles Herrmann, Junhwa Hur, Varun Jampani, Trevor Darrell, Forrester Cole, Deqing Sun, and Ming-Hsuan Yang. Monst3r: A simple approach for estimating geometry in the presence of motion. *arXiv preprint arxiv:2410.03825*, 2024. 1, 2, 6
- [42] Songyan Zhang, Yongtao Ge, Jinyuan Tian, Guangkai Xu, Hao Chen, Chen Lv, and Chunhua Shen. Pomato: Marrying pointmap matching with temporal motion for dynamic 3d reconstruction. *arXiv preprint arXiv:2504.05692*, 2025. 2, 6
- [43] Shangzhan Zhang, Jianyuan Wang, Yinghao Xu, Nan Xue, Christian Rupprecht, Xiaowei Zhou, Yujun Shen, and Gordon Wetzstein. Flare: Feed-forward geometry, appearance and camera estimation from uncalibrated sparse views. arXiv preprint arXiv:2502.12138, 2025. 2
- [44] Zhoutong Zhang, Forrester Cole, Zhengqi Li, Michael Rubinstein, Noah Snavely, and William T Freeman. Structure and motion from casual videos. In *European Conference on Computer Vision*, pages 20–37. Springer, 2022. 1, 2
- [45] Yang Zheng, Adam W. Harley, Bokui Shen, Gordon Wetzstein, and Leonidas J. Guibas. Pointodyssey: A large-scale synthetic dataset for long-term point tracking. In *ICCV*, 2023. 6
- [46] Dong Zhuo, Wenzhao Zheng, Jiahe Guo, Yuqi Wu, Jie Zhou, and Jiwen Lu. Streaming 4d visual geometry transformer. arXiv preprint arXiv:2507.11539, 2025. 2

VGGT4D: Mining Motion Cues in Visual Geometry Transformers for 4D Scene Reconstruction

Supplementary Material

6. Empirical Analysis of Attention Layers

We analyze how the decoder layers of VGGT encode dynamic content. Our findings motivate the specific design choices in our dynamic cue extraction module.

6.1. Gram Similarity vs. Standard Attention

We first compare standard attention maps with our proposed Gram similarity statistics. As shown in Figs. 7 and 8, we visualize the statistics (mean and variance) for each decoder layer. Here, *ref* denotes the reference frame and *src* denotes a source frame sampled from the temporal window.

Standard Attention (QK^{\top}) . Inspecting the $Q_{\rm ref}K_{\rm src}$ column reveals that standard attention is dominated by semantic activations. Motion cues are barely visible. This also explains why applying Easi3R to VGGT fails: the strong semantic bias in QK^{\top} washes out dynamic motion signals. Gram Similarity $(QQ^{\top}$ and $KK^{\top})$. In contrast, the Gram similarities (columns $Q_{\rm ref}Q_{\rm src}$ and $K_{\rm ref}K_{\rm src}$) make physically dynamic regions salient. This confirms that while motion cues are suppressed in standard attention, they are preserved in the self-similarity of queries and keys.

6.2. Layer-wise Dynamic Cues

Based on the Gram similarity patterns, we identify three distinct regimes across the decoder layers:

- Shallow layers (e.g., layer 1). In the $K_{\rm ref}K_{\rm src}$ column, the model shows a strong semantic bias. Foreground objects stand out clearly from the background, regardless of their motion state.
- Middle layers (e.g., layers 4–8). As seen in the Q_{ref}Q_{src} column, VGGT begins to encode motion variability. The Gram similarities computed from Q vectors over the temporal window sharpen the contrast between truly dynamic regions and the static background.
- Deep layers (e.g., layers 18–22). In the $Q_{\rm ref}Q_{\rm src}$ column, spatial priors dominate. This suppresses noisy responses from earlier layers, resulting in sharper and more stable boundaries.

6.3. Ineffectiveness of Camera Token Attention

A potential alternative to our method is relying on the camera token to identify dynamic regions. We test this hypothesis in Fig. 9. While the camera token focuses on dynamic regions in shallow layers (Layer 1), it fails to suppress them in deep layers (Layer 18). The actor's body receives attention comparable to the static background. This indicates that

deep camera-token attention is unreliable for dynamic disentanglement, justifying our explicit mining of Gram similarity cues.

6.4. Explanation of the Design

Hypothesis on gram similarity. We hypothesize that the Gram similarity $(QQ^{\top} \text{ or } KK^{\top})$ serves as a superior amplifier for dynamic cues compared to the standard crossattention (QK^{\top}) . The standard attention mechanism computes interactions between Ouery and Key vectors, which originate from distinct projection heads to perform semantic alignment. The inherent distributional gap between these heterogeneous vectors tends to overshadow the subtle feature variations induced by object motion, rendering dynamic signals nearly invisible. In contrast, the Gram similarity operates on vectors within the same latent distribution. Without the interference of cross-projection discrepancies, the feature bias introduced by dynamics becomes the dominant source of variance. Consequently, the Gram operation effectively magnifies these intra-distributional differences, making dynamic regions significantly more salient than the static background.

Why camera token is unreliable? One might expect the global camera token in deep layers to strictly attend only to static regions for robust pose estimation. However, we observe that Transformer-based foundation models achieve robustness through soft aggregation rather than hard exclusion. The model learns to tolerate a certain degree of dynamic noise (outliers) within its massive context window to solve the global pose optimization. As a result, the camera token does not explicitly 'zero out' dynamic regions but rather down-weights them subtly or mixes them into the context. This leads to ambiguous attention maps that are insufficient for generating precise, binary dynamic masks.

7. Implementation Details

7.1. Hyperparameters

We provide the specific hyperparameters used in our pipeline in Tab. 7.

7.2. Dynamic Cue Extraction & Memory Optimization

As detailed in Sec. 6, we combine cues from three layer groups. We extract $w_{\rm shallow}$ from Layer 1 for strong semantics. We extract $w_{\rm middle}$ from Layers 4–8 to capture motion variance. Finally, we extract $w_{\rm deep}$ from Layers 18–22 to utilize spatial priors for outlier suppression.

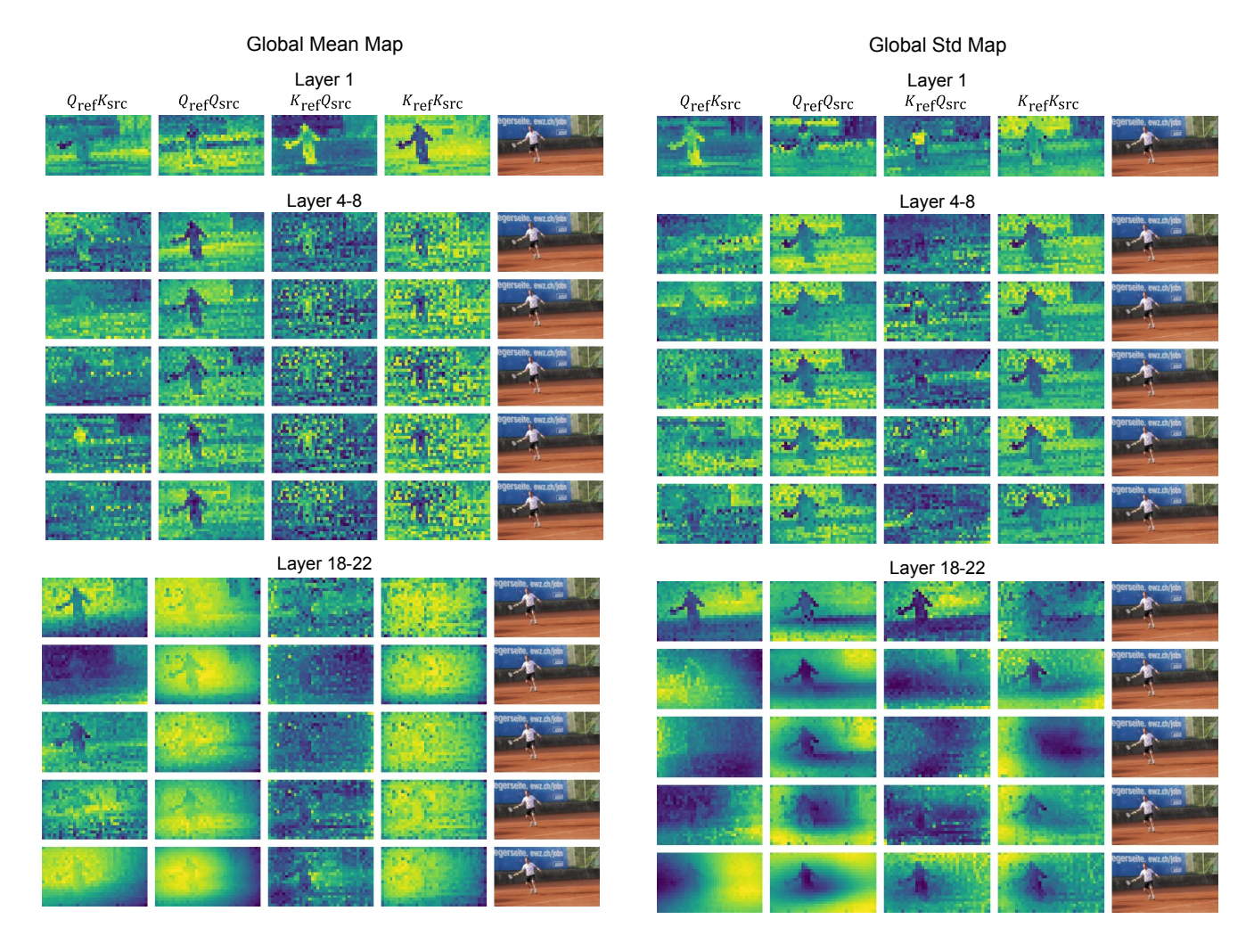


Figure 7. Mean Gram similarity across decoder layers. We visualize Gram similarity maps averaged over a temporal window. The $Q_{\rm ref}K_{\rm src}$ column shows the standard attention map (QK^\top) . Note that motion cues are faint in standard attention but distinct in Gram similarities (QQ^\top,KK^\top) .

Parameter	Value
Temporal Window	6 source frames (stride 2)
Layers for $w_{\rm shallow}$	Layer 1
Layers for w_{middle}	Layers 4–8
Layers for w_{deep}	Layers 19–20 (Var), 18–22 (Mean)
Early-stage Masking Layers	Layers 1–5
SOR Neighbors (k)	20

Table 7. **Hyperparameter settings.** Key parameters for cue extraction and refinement.

2.5

SOR Std. Dev. Mult. (σ)

To define the threshold α , which is used in Sec. 3.3 to obtain dynamic mask, we use VGGT's ViT backbone to extract image features and apply k-means clustering to group

Figure 8. Variance of Gram similarity across decoder layers. We visualize the variance of Gram similarity. Similar to the mean statistics, Gram similarities capture motion variance more effectively than standard attention $(Q_{\rm ref}K_{\rm src})$.

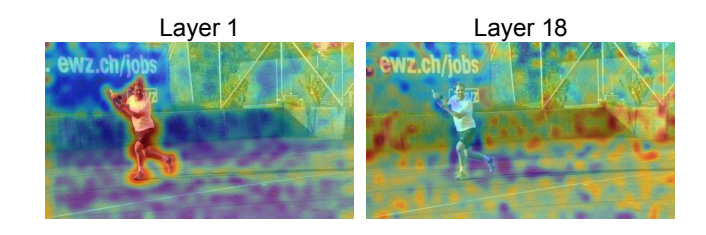


Figure 9. Camera-to-image attention limitations. We visualize attention from the camera token to image tokens. In Layer 18, the camera token fails to suppress the moving actor, treating it similarly to the static background. This confirms that camera tokens are insufficient for robust dynamic masking.

tokens across frames. We verify the dynamic score of each cluster and use Otsu's algorithm to determine the optimal separation threshold.

Memory Optimization. VGGT uses PyTorch's Scaled Dot Product Attention (SDPA) for efficiency. Explicitly computing the full Gram matrix QK^{\top} scales quadratically with token count $(O(N^2))$, which would cause Out-Of-Memory (OOM) errors given the thousands of tokens in multi-view inputs. To resolve this, we compute per-frame Gram similarities in-place within the attention layer. This avoids materializing the massive full matrix and keeps memory usage linear with respect to the number of frames.

7.3. Mask Refinement

Raw masks from 3D foundation models often contain outliers ("floaters"). These artifacts degrade the projection-based refinement. We first apply Statistical Outlier Removal (SOR) to the point cloud to filter noise. Next, we cluster the remaining points and average the projection gradients within each cluster. This aggregation stabilizes the gradient signal, preventing isolated outliers from triggering false positives in the dynamic classification.

7.4. Early-Stage Masking

During inference, we apply the dynamic masks only to layers 1-5. We suppress the key (K) vectors of dynamic tokens in these layers. This prevents query (Q) vectors from attending to dynamic regions early in the network, preserving the geometric consistency of deeper layers.

8. Additional Experiments

8.1. Ablation Study on Dynamic Map Components

We validate the contribution of each term in Eq. (5) (Main Paper). As shown in Tab. 8, $w_{\rm shallow}$ and $w_{\rm middle}$ provide the primary motion signals. However, performance drops significantly without $w_{\rm deep}$, confirming its role in suppressing residual outliers.

Method	DAVIS-2016						
1/1001100	JM↑	JR↑	FM↑	FR↑			
w/o w _{shallow}	54.15	62.44	46.43	44.27			
w/o $w_{ m middle}$	56.13	57.12	44.07	41.90			
w/o $w_{ m deep}$	46.85	48.89	41.52	45.30			
w/o refinement	<u>59.74</u>	<u>73.10</u>	<u>50.64</u>	<u>58.30</u>			
Ours	62.12	76.80	56.04	67.49			

Table 8. **Ablation on dynamic mask estimation.** We evaluate the contribution of each component. Note that the "w/o" variants are evaluated before the refinement stage to isolate the impact of the cue extraction.

8.2. Zero-shot vs. Trained 2D Segmentation

We compare our method against FlowSAM, a strong 2D video segmentation baseline. FlowSAM lacks 3D spatial reasoning and typically requires ground-truth supervision (Hungarian matching) for evaluation. For a fair comparison, we adapt FlowSAM to a zero-shot setting.

As shown in Tab. 9, our training-free approach outperforms the trained FlowSAM baseline. This demonstrates that leveraging the implicit 3D/4D priors in VGGT yields better temporal consistency than pure 2D video analysis.

Method	DAVIS-2016						
1/10/11/04	JM↑	JR↑	FM↑	FR↑			
FlowSAM (zero-shot)	54.53	56.86	52.48	52.97			
DAS3R	41.13	38.67	44.50	36.94			
Easi3R _{dust3r}	50.10	55.77	43.40	37.25			
Easi3R _{monst3r}	<u>54.93</u>	<u>68.00</u>	45.29	47.30			
Ours	62.12	76.80	56.04	67.49			

Table 9. **Dynamic object segmentation comparison.** Our method outperforms the trained 2D baseline FlowSAM in a zero-shot setting.

9. Limitations

While our method achieves robust 4D reconstruction without training, it has limitations. First, computing Gram similarities adds computational overhead compared to single-pass inference. Second, our mask refinement depends on the quality of the initial depth estimates from VGGT. If the backbone misestimates depth (e.g., blending foreground and background), the projection gradients become unreliable. Finally, our refinement assumes rigid motion for projection checks, which may struggle with highly non-rigid or fluid deformations. Future work will focus on optimizing efficiency and handling non-rigid dynamics.